MLSE Post-Detection for ISI Mitigation and Synchronization in UWB Low Complexity Receivers

Florian Troesch and Armin Wittneben
Communication Technology Laboratory, ETH Zurich, 8092 Zurich, Switzerland
Email: {troeschf, wittneben}@nari.ee.ethz.ch

***Abstract*— A wireless body area network with an average throughput of 1 Mbps is considered based on ultra-wideband pulse position modulation. For a long battery autonomy, a low duty cycle operation of the nodes and thus, a high peak data rate is essential. Due to the moderate path loss, a peak data rate in excess of 50 Mbps is feasible within the Federal Communications Commission's transmit power constraints. However, with current low complexity pulse position detectors, such as the energy detector, the peak data rate is constrained to much lower values, because they are very sensitive to intersymbol interference. To overcome this constraint a simple post-detection maximum-likelihood sequence estimator is introduced which significantly reduces the impact of intersymbol interference. The same maximum likelihood sequence estimator is then used to replace cumbersome synchronization algorithms at the expense of slight performance losses.**

I. Introduction

Recently, ultra-wideband (UWB) wireless body area networks (WBAN) gained much interest due to a multitude of attractive applications, such as wireless health monitoring or ubiquitous computing. In a WBAN, a number of small nodes are placed directly on the human body or very close to it. Since WBAN nodes get their power from rechargeable batteries or by energy harvesting, it is inevitable that they are extremely energy efficient. To meet such energy requirements, a low duty cycle operation of the nodes and thus a high peak data rate is essential. Due to the moderate path loss in WBANs [1], a peak data rate in excess of 50 Mbps is feasible within the Federal Communications Commissions's (FCC) transmit power constraints [2]. However, the peak data rate is constrained to much lower values with current low complexity energy detectors as they are very sensitive to intersymbol interference (ISI). Furthermore, mentioned energy requirements ask for power efficient synchronization algorithms. However, with UWB impulse radio (UWB-IR) synchronization can be a cumbersome task due to the peaky nature of the transmit signal in time domain.

For both increased peak data rate and simple synchronization, we propose a simple post-detection maximum likelihood sequence estimator (MLSE) that bases its decision on the output of an analog energy detector frontend. The frontend basically consists of a squaring device and an integrate-and-dump circuit, clocked at twice the symbol rate, as shown in Fig.2. The MLSE has no direct access to the receive signal. Hence, non-linear cross-correlation terms are not avoidable. For the investigated scenario, it can be implemented by a basic Viterbi algorithm of only a few states. The proposed MLSE is shown to be a very efficient and simple approach to both overcome the effect of ISI at high data rates and to replace complex synchronization algorithms. For synchronization, a clock offset between transmitter and receiver is transferred into an equivalent ISI problem, which is then solved by the MLSE.

While their exists a wide literature on MLSE for energy detectors in the area of optical communications, the optical channel is generally modeled linear in energy [3], [4]. There exist different works on MLSE for ISI mitigation in UWB-IR PPM systems, but most of them treat linear receiver structures, equalizing overall channel impulse responses (CIR). This is too complex for WBAN receivers. In [5], a decision feedback equalizer for UWB-IR on-off keying is investigated and [6] considers convolutional codes for non-linear UWB-IR detection. In both papers non-linear cross-correlation terms are either neglected or avoided, basically resulting in a linear model, again.

The main contribution of this work is the application of the MLSE principle to the non-linear output of an analog UWB BPPM frontend, explicitly taking into account non-linear cross-correlation terms and data dependent noise variances. For weak ISI, i.e., one slot interference, first results were presented in [7], where proposed MLSE was compared to several symbol-wise detectors based on different amount of partial channel state information. The presented MLSEs have very reduced CSI, i.e., the fraction of energy falling into different PPM slots, work at symbol rate with only a few states, and all the same, achieve good or even full ISI cancelation. Significant performance differences between MLSEs working on PPM slot and symbol level are demonstrated. Finally, proposed MLSEs are investigated as replacement for complex synchronization algorithms.

The remainder of this paper is organized as follows. In Section II, considered system model is introduced and the output of the analog energy detector frontend is derived. The MLSE post-detection is presented in Section III. Efficient optimal and suboptimal implementations are discussed in Section V. Performance results are shown in Section VI and VII with respect to ISI mitigation and synchronization, respectively.

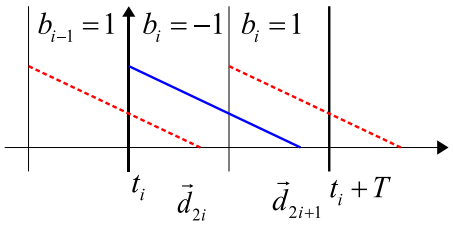

Fig. 1. ISI due to large channel excess delay

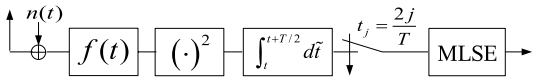

Fig. 2. Block diagram of analog receiver frontend.

II. The Analog Frontend

We consider a UWB-IR system with binary pulse position modulation (BPPM). Moreover, it is assumed that only one pulse is transmitted per symbol, which is reasonable for short range communication in WBANs due to moderate path loss [1]. Time-hopping is omitted for convenience of the derivation but can be easily included for real systems. The nominal pulse period T determines a BPPM frame. Each frame contains one transmit pulse. Depending on the BPPM symbol value, the pulse is either in the first or the second BPPM half-frame of duration $T/2$. Due to a large maximum excess delay ISI occurs as illustrated in Fig. 1.

By mapping the i-th BPPM symbol to a binary vector, according to:

$$b_i = -1 \rightarrow \vec{x}_i = [\ x_{2i} \quad x_{2i+1}\ ]^T = [\ 1 \quad 0\ ]^T \quad (1)$$

$$b_i = 1 \rightarrow \vec{x}_i = [\ x_{2i} \quad x_{2i+1}\ ]^T = [\ 0 \quad 1\ ]^T, \quad (2)$$

the discrete baseband description of the transmit signal during the j-th BPPM half-frame equals:

$$\vec{c}_j = x_j \vec{w}, \quad (3)$$

where $\vec{w}$ is the discrete description of the transmit waveform at twice the Nyquist rate, which is necessary to keep the discrete model correct after the squaring device of the receiver. Its energy is set to $1/(4B)\vec{w}^H\vec{w} = E_\mathrm{b}$.

The analog energy detector frontend is shown in Fig. 2. The noisy receive signal is filtered by a bandpass filter $f(t)$ and passed through a squaring device. The squared output signal is then integrated-and-dump at rate $2/T$. The bandbass filter is assumed to be ideal and its band is chosen such that the receive signal of bandwidth B passes unchanged.

During the j-th BPPM half-frame, the receive signal after the bandpass filter is described by:

$$\vec{d}_j = \sum_{l=0}^{L-1} x_{j-l}\vec{h}_l + \vec{n}_j, \quad (4)$$

where $\vec{h}_l$ is the l-th part of the CIR according to

$$\vec{h} = \left[\ \vec{h}_0^T \quad \vec{h}_1^T \quad \ldots \quad \vec{h}_{L-1}^T\ \right]^T. \quad (5)$$

Totally, there are L pieces in $\vec{h}$, each of duration $T/2$. $\vec{n}_j$ contains zero-mean additive white Gaussian noise (AWGN) with $\mathcal{E}\left\{\vec{n}_j\vec{n}_j^H\right\} = \sigma^2\mathbf{I}$, where $\mathbf{I}$ is the identity matrix. The j-th sample after the integration unit can be written as:

$$y_j = \vec{d}_j^H\vec{d}_j = \left\|\sum_{l=0}^{L-1} x_{j-l}\vec{h}_l + \vec{n}_j\right\|^2 \quad (6)$$

$$= \left\|\sum_{l=0}^{L-1} x_{j-l}\vec{h}_l\right\|^2 + 2\mathrm{Re}\left\{\left(\sum_{l=0}^{L-1} x_{j-l}\vec{h}_l\right)^H \vec{n}_j\right\}$$

$$+ \vec{n}_j^H\vec{n}_j \quad (7)$$

$$= s_j + p_j + q_j, \quad (8)$$

where s_j is the signal component and p_j is a Gaussian random variable arising from the mixed signal-noise term with zero mean and variance:

$$\sigma_{p_j}^2 = 2\sigma^2\left(\sum_{l=0}^{L-1}\sum_{k=0}^{L-1} x_{j-l}x_{j-k}\vec{h}_l^H\vec{h}_k\right). \quad (9)$$

The squaring device causes an additional non-linear noise term q_j in y_j, which is χ^2 distributed with $2L$ real degrees of freedom. Due to the large system bandwidth and a long integration duration, $2L$ is large. Hence, the law of large numbers [2] is applied to approximate q_j as a Gaussian random variable with expectation and variance:

$$m_{q,j} = L\sigma^2 \quad (10)$$

$$\sigma_{q,j}^2 = 2L\sigma^4. \quad (11)$$

With this, y_j is expressed as

$$y_j = s_j + z_j, \quad (12)$$

where z_j is a Gaussian random variable with mean and variance according to:

$$m_{z,j} = L\sigma^2 \quad (13)$$

$$\sigma_{z,j}^2 = 2\sigma^2\left(\sum_{l=0}^{L-1}\sum_{k=0}^{L-1} x_{j-l}x_{j-k}\vec{h}_l^H\vec{h}_k\right) + 2L\sigma^4. \quad (14)$$

III. MLSE Backend

Differently from typical energy detector backends doing symbol-wise detection, the considered MLSE backend estimates overall sequences, i.e., it works on the frontend output vector:

$$\vec{y} = [y_0, y_1, \ldots, y_{2K+L-2}]^T, \quad (15)$$

where K is the number of BPPM symbols contained in the observed sequence. The vector $\vec{y}$ contains $2K + L - 1$ entries, whereby, the last $L-1$ entries are caused by a large maximum excess delay.

Defining the matrix $\mathbf{V} = [\ \vec{h}_0 \quad \vec{h}_1 \quad \ldots \quad \vec{h}_{L-1}\ ]$, the CSI $\mathcal{C}_1$ of the first MLSE (MLSE1) is described by:

$$\mathcal{C}_1 \quad = \quad \mathbf{V}^H\mathbf{V}, \tag{16}$$

which can be estimated by only a few pilot symbols. The number of required pilots is further decreased by applying the assumption:

$$\mathcal{C}_2 = \mathbf{V}^H\mathbf{V} \stackrel{!}{=} \mathbf{I}\left[\ \vec{h}_1^H\vec{h}_1 \quad \vec{h}_2^H\vec{h}_2 \quad \ldots \quad \vec{h}_L^H\vec{h}_L\ \right]^T. \tag{17}$$

This is taken as the CSI of the second MLSE (MLSE2). Hence, MLSE2 assumes that $\vec{h}_j$ and $\vec{h}_i$ are orthogonal for $i \neq j$. Defining $\vec{x}$ as the transmitted vector

$$\vec{x} \quad = \quad [x_0, x_1, \ldots, x_{2K-1}]^T \tag{18}$$

with $x_j \in \{0, 1\}$ half a symbol according to (1) and (2), the MLSE picks the vector $\hat{\vec{x}}$ which maximizes the probability that $\vec{y}$ was received given a certain CSI $\mathcal{C}_i$ and $\hat{\vec{x}}$ [8]:

$$\underset{\hat{\vec{x}}}{\text{argmax}}\ p\left(\vec{y}|\hat{\vec{x}}, \mathcal{C}_i\right). \tag{19}$$

Although, the variance of the random variable z_j depends on the past, z_j is independent of the past, if y_{j-1} is known. Therefore, application of the Markov Chain rule leads to:

$$p\left(\vec{y}|\hat{\vec{x}}, \mathcal{C}_i\right) \quad = \quad \prod_{j=2}^{2K+L} p\left(y_{2K+L-j}|y_{2K+L-1-j}, \cdots \right.$$
$$\left., y_{2K+1-j}, \hat{x}_{2K+L-j}, \mathcal{C}_i\right), \tag{20}$$

whereby $y_{-1} = y_{-2} = \ldots = y_{-L+1} = 0$. Hence, we can write the MLSE as a simple Viterbi algorithm:

$$\begin{aligned} & \underset{\hat{\vec{x}}}{\text{argmax}} \log\left\{p\left(\vec{y}|\hat{\vec{x}}, \mathcal{C}_i\right)\right\} \\ = \quad & \underset{\hat{\vec{x}}}{\text{argmin}} \sum_{j=0}^{2K+L-2} \frac{|y_j - \hat{s}_j - m_{z,j}|^2}{2\sigma_{z,j}^2} + 0.5\log\left(2\pi\sigma_{z,j}^2\right) \\ = \quad & \underset{\hat{\vec{x}}}{\text{argmin}} \sum_{j=0}^{2K+L-2} m(y_j, \hat{x}_j, \zeta_j), \end{aligned} \tag{21}$$

with ζ_j, the state of the Viterbi algorithm at time instance j. The partial CSI $\mathcal{C}_1$ or $\mathcal{C}_2$ is required for the construction of $m_{z,j}$, $\sigma_{j,z}^2$ as well as $\hat{s}_j$ according to (12).

IV. Efficient Optimal and Suboptimal MLSE Implementation

While the Viterbi describe in (21) is a possible approach to cancel ISI, its implementation is somewhat cumbersome as only a subset of all possible trellis is allowed due to the cyclic property of the codewords $\vec{x}_j$. This can be avoided efficiently by working on the vectors $\vec{x}_j$ rather than on half-frame level, leading to:

$$\begin{aligned} & \underset{\hat{\vec{x}}}{\text{argmin}} \sum_{i=0}^{S-1} \left[\frac{|y_{2i+1} - \hat{s}_{2i+1} - m_{z,2i+1}|^2}{2\sigma_{z,2i+1}^2}\right. \\ & \left. + \frac{|y_{2i} - \hat{s}_{2i} - m_{z,2i}|^2}{2\sigma_{z,2i}^2} + 0.5\log\left(4\pi^2\sigma_{z,2i}^2\sigma_{z,2i+1}^2\right)\right] \end{aligned} \tag{22}$$

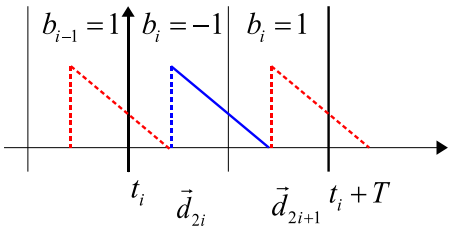

Fig. 3. ISI due to synchronization error.

with $S = \lceil(2K + L - 1)/2\rceil$. This reduces the number of states by a factor of two and more important makes the Viterbi transitions time-invariant.

A simplified algorithm works on PPM symbol level, i.e., on the difference $y_{2i+1} - y_{2i}$. But this is not a sufficient statistics, when ISI occurs and therefore, important information for the sequence estimation is lost leading to a suboptimal receiver. All the same, the approach is important as in certain receivers, it might not be possible to access half-frame samples but only the BPPM symbols. The suboptimal MLSE applying $\mathcal{C}_1$ is called MLSE3 and the one based on $\mathcal{C}_2$ is called MLSE4.

V. MLSE for Synchronization

By now ISI arising from a large channel excess delay was considered. But ISI can also occur due to an offset between transmitter and receiver clock, even if the excess delay is small. This is demonstrated in Fig. 3. Assuming a free running clock at the receiver, the channel energy spreads over two BPPM half-frames. Hence, the synchronization mismatch is simply considered as a source of ISI, which can be canceled by proposed MLSE. With this, complex synchronization algorithms can be replaced by a simple MLSE based on following CSI:

$$\mathcal{C}_3 \quad = \quad \mathbf{B}^H\mathbf{B}, \tag{23}$$

with matrices:

$$\mathbf{B} = \left[\ \vec{0} \quad \ldots \quad \vec{0} \quad \vec{h}_0 \quad \vec{h}_1 \quad \ldots \quad \vec{h}_L \quad \vec{0} \quad \ldots \quad \vec{0}\ \right]. \tag{24}$$

In general, a clock offset increases the number of ISI half-slots by one. For a channel duration below 10 ns the MLSE has to work with two states, if the sampling clock of the analog frontend is free running. As the rate of the sampler is exactly the inverse of the integration duration $2/T$, the analog frontend is integrating continuously, and therefore, no energy can be lost between slots.

VI. Performance Results: ISI

We compare the performance of the MLSE receivers derived above with the symbol-wise energy detector ignoring any ISI (ED) as well as with the energy detector that does not encounter any ISI, i.e., the matched filter bound (MFB). This is done by means of bit error rate (BER) simulations. The BER is plotted over the signal-to-noise ratio (SNR) E_b/N_0, where E_b denotes the energy per bit and $N_0/2$ is the noise power

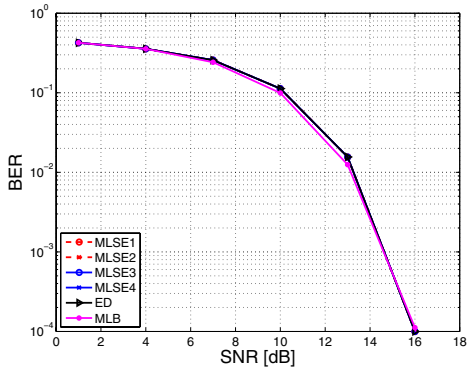

Fig. 4. BER in case of no ISI (Max. Excess Delay $= 8$ ns)

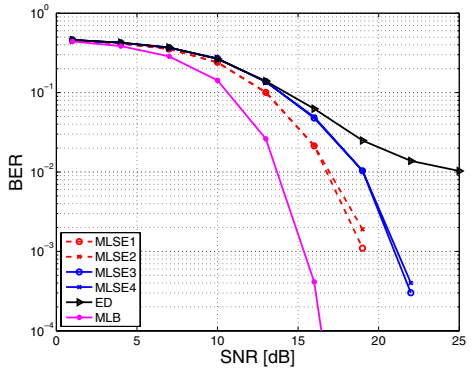

Fig. 5. BER for weak ISI (Max. Excess Delay $= 14$ ns)

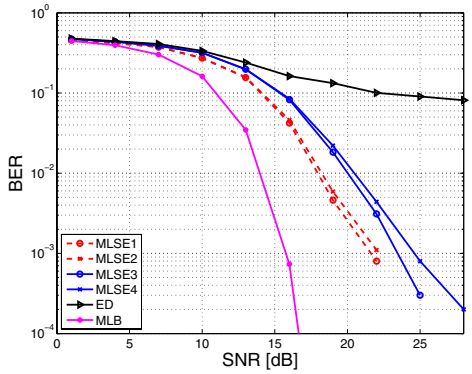

Fig. 6. BER for strong ISI (Max. Excess Delay $= 17$ ns)

spectral density. We assume uniformly distributed channel taps, which is a worst case average power delay profile with respect to ISI. To achieve a data rate of 50 Mbps with BPPM, one bit has to be transmitted every 20 ns. Hence, one BPPM frame has a duration of $T = 20$ ns, i.e., one BPPM slot has a duration of 10 ns and ISI occurs for CIRs with a duration of more than 10 ns. We consider the four cases that no ISI, weak ISI, strong ISI and very strong ISI occurs. In the case of no ISI the CIR has a duration of 8 ns, for weak ISI it is 14 ns, for strong ISI 17 ns, and for very strong ISI 25 ns.

a) No ISI: The BER curves in case of no ISI are shown in Fig. 4. In absence of ISI, the MLSE corresponds to a simple symbol-wise energy detector. Furthermore, the difference $y_{2i+1} - y_{2i}$ constitutes a sufficient statistics. Thus, the performance of the four MLSEs and the ED are all equal to the MFB.

b) Weak ISI: For the case of weak ISI, with a CIR duration of 14 ns, the performance results are shown in Fig. 5. It is apparent that the symbol-wise energy detector experiences a strong performance degradation. Due to the ISI, the influence of the noise on the BER performance is not dominant for high E_b/N_0 values and the BER curve of the ED approaches an error floor at 10^{-2}. The performance of MLSE1 and MLSE2 on the one hand and MLSE3 and MLSE4 on the other hand are similar, pointing out that for weak ISI cross-correlation terms are neglectable. Furthermore, already for weak ISI a significant performance loss of MLSE3 and MLSE4 appears due to their suboptimality. Still, all four MLSEs show very good performance with respect to the symbol-wise detector.

c) Strong ISI: The BER curves for strong ISI are plotted in Fig. 6 for a CIR of 17 ns. The performance of the symbol-wise energy detector further decreases, while the performance of the MLSEs degrades only slightly by approximately 2 dB. The performance degradation of the MLSEs arises from a reduced minimal free distance between different possible receive sequences. The significance of the cross-correlation terms ignored by MLSE2 and MLSE4 has slightly increased with stronger ISI. For the MSLE4, an error floor at higher SNR was expected pointing out that MLSE4 does not cancel ISI entirely, but even for strong ISI, an error floor is hardly visible. Hence, although working on symbol level and ignoring cross-correlation terms, not too much information is lost with respect to ISI cancelation. All the same, the approach experiences significant performance losses for strong ISI, but is a promising candidate for moderate ISI.

d) Very strong ISI: BER curves for a CIR of duration of 25 ns are shown in Figure 7. As expected, MLSE2 and MLSE4 do not cancel ISI well anymore and they experience an error floor at high SNR. Hence, for very strong ISI cross-correlations have to be taken into account to achieve good ISI cancelation. MLSE3 and especially MLSE1 show promising performance. MLSE3 working on symbol level is significantly worse than MLSE1, but still cancels ISI quite good.

VII. Performance Results: Synchronization

In this section, the MLSE performance is investigated, if ISI arises from a clock offset between transmitter and receiver. In Fig. 8, performances are shown for an unsynchronized system, where the maximum excess delay equals 8 ns. Hence, ISI occurs only due to a clock offset. It is evident that the symbol-wise detector can not decode due to the clock offset varying between 0 and several integration durations. If no synchronization mismatch was present, the performance of the MLSEs would achieve the matched filter bound as in Fig. 4. Hence, for short CIRs, the application of proposed MLSE as a simple and efficient mean for synchronization leads to a performance loss between 4 and 8 dB, depending

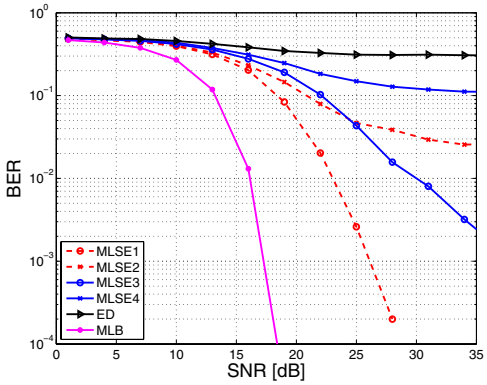

Fig. 7. BER: Very strong ISI (Max. Excess Delay $= 25$ ns)

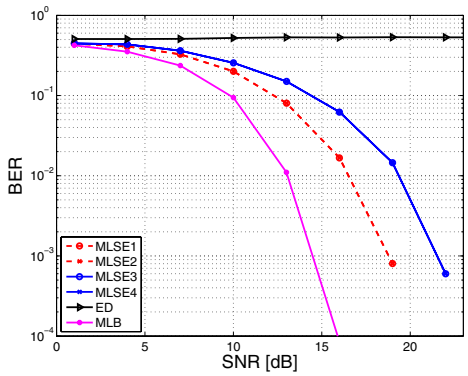

Fig. 8. MLSE for synchronization (Max. Excess Delay $= 8$ ns)

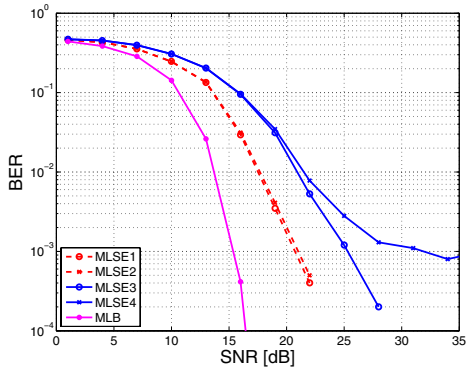

Fig. 9. MLSE for synchronization (Max. Excess Delay $= 14$ ns)

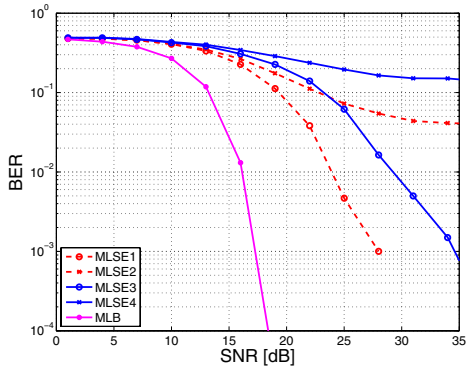

Fig. 10. MLSE for synchronization (Max. Excess Delay $= 25$ ns)

on the MLSE realization. Although a loss of 8 dB is certainly significant, the MLSE constitutes an interesting approach as no additional synchronization is necessary. For considered scenario, cross-correlation terms are neglectable and hence, MSLE1 and MLSE2 on the one hand and MLSE3 and MLSE4 on the other hand show equal performance. Also for slight and strong ISI, with a CIR duration of 14 ns and 25 ns, shown in Fig. 9 and Fig. 10, respectively, the unsynchronized MLSE approach shows good results. While, MLSE2 and MLSE4 experience an error floor, it turns out that even for strong ISI, the two MLSEs considering cross-correlation terms cancel occurring ISI, almost entirely. The performance loss with respect to Fig. 7 is marginal!

VIII. Conclusions

A promising MLSE approach was presented, which is working on the output of an analog energy detector frontend. The MLSE works with very little CSI, i.e., the amount of energy falling into a certain BPPM half-frame, and can be implemented as a Viterbi algorithm of only a few states. Depending on the specific MLSE realization, presented approach is capable to cancel strong ISI which spreads uniformly over several BPPM half-frames. For moderate ISI, also presented simplified MLSEs cancel ISI effectively. While the overhead required for the slightly more complex MLSE1 seems outweighing its performance gains at weak and moderate ISI, it is certainly a worthwhile approach for strong and very strong ISI. Finally, it was demonstrated that complex synchronization algorithms can be omitted by using one of the proposed simple MLSEs at the expense of a reduced BER performance.

References

[1] T. Zasowski, G. Meyer, F. Althaus, and A. Wittneben, "UWB signal propagation at the human head," *IEEE Trans. on MTT*, vol. 54, no. 4, April 2006.

[2] F. Troesch, F. Althaus, and A. Wittneben, "Modified pulse repetition coding boosting energy detector performance in low data rate systems," in *IEEE Int. Conf. Ultra-Wideband (ICU)*, Zurich, Switzerland, Sept. 5 – 8, 2005.

[3] J. R. Barry, "Sequence detection and equalization for pulse-position modulation," in *Proc. ICC*, vol. 3, New Orleans, LA, May 1–5, 1994, pp. 1561 – 1565.

[4] A. Klein and C. Johnson, "MMSE Decision Feedback Equalization of Pulse Position Modulated Signals," in *Proc. ICC*, Ithaca, NY, US, 20–24 June 2004.

[5] M. Sahin and H. Arslan, "Inter-symbol interference in high data rate UWB communications using energy detector receivers," in *IEEE Int. Conf. Ultra-Wideband (ICU)*, Zurich, Switzerland, Sept. 5 – 8, 2005.

[6] A. R. Forouzan and M. Abtahi, "Application of convolutional error correcting codes in ultrawideband M-ary PPM signaling," *IEEE Microwave and Wireless Components Letter*, vol. 13, no. 8, pp. 308 – 310, Aug. 2003.

[7] T. Zasowski, F. Troesch, and A. Wittneben, "Partial channel state information and intersymbol interference in low complexity UWB PPM detection," in *IEEE Int. Conf. Ultra-Wideband (ICUWB)*, Waltham, MA, Sept. 25 – 27, 2006.

[8] G. D. Forney, "Maximum-likelihood sequence estimation in the presence of intersymbol interference," *IEEE Trans. Inform. Theory*, vol. 18, no. 3, pp. 363–378, May 1972.